coatings

MDPI

Article

Enhanced Protective Performance of Carbon Nanotube-Reinforced Waterborne Epoxy Zinc-Rich Coatings for Corrosion Protection of Steel Structures

Xueling Huang [1], Chun Yang [1], Junyu Chen [1], Xinglong Qiao [2], Shuguang Zhang [2,*] and Dan Song [2,*]

[1] State Grid Wuxi Power Supply Company, Wuxi 214000, China; hxl_wx@sina.com (X.H.); yangchun@js.sgcc.com.cn (C.Y.); chen_junyu1986@126.com (J.C.)
[2] College of Materials Science and Engineering, Hohai University, Nanjing 211100, China; 221608010037@hhu.edu.cn
* Correspondence: shuguang0502@163.com (S.Z.); songdancharls@hhu.edu.cn (D.S.)

Abstract: Carbon nanotube-reinforced waterborne epoxy zinc-rich coatings were developed by modifying waterborne epoxy zinc-rich formulations with varying amounts of carbon nanotubes (CNTs), to improve the coatings' corrosion resistance and their protection for Q355b steel in environments rich in chlorides. A detailed investigation of the microstructural changes in the coatings prior to and following corrosion was conducted through FTIR, SEM, XRD, and XPS analytical techniques. The effectiveness of these innovative coatings in providing corrosion protection for Q355b steel in chloride conditions was assessed via electrochemical corrosion methodologies and neutral salt spray testing. The results indicate that an increase in the CNT concentration led to an initial enhancement in the corrosion resistance of the coatings, followed by a decrease, with optimal performance noted at 0.3 wt.% CNTs. During the electrochemical evaluations, the open circuit potential (OCP) of the coating containing 0.3 wt.% CNTs remained stable below the critical threshold of −0.78 V for an extended period, indicating sustained cathodic protection. In comparison to the coatings with CNT concentrations (wt.%) of 0.1, 0.5, 0.7, and 1.0, the coating with 0.3 wt.% CNTs demonstrated the lowest corrosion current density, measured at 0.0322 μA/cm^2. Further validation of its exceptional corrosion resistance was provided by the 240 h neutral salt spray tests. This performance can be linked to the capability of the CNTs to improve electrical conductive connectivity between the zinc particles and the Q355b steel substrate beneath them, subsequently enhancing both the cathodic protection of the coating and its physical shielding effectiveness.

Keywords: waterborne epoxy zinc-rich coatings; carbon nanotubes; corrosion resistance; corrosion mechanism; cathodic protection

Citation: Huang, X.; Yang, C.; Chen, J.; Qiao, X.; Zhang, S.; Song, D. Enhanced Protective Performance of Carbon Nanotube-Reinforced Waterborne Epoxy Zinc-Rich Coatings for Corrosion Protection of Steel Structures. *Coatings* **2024**, *14*, 1493. https://doi.org/10.3390/coatings14121493

Academic Editor: Francesco Di Quarto

Received: 6 November 2024
Revised: 23 November 2024
Accepted: 25 November 2024
Published: 27 November 2024

1. Introduction

Zinc-rich coatings are widely applied in various corrosive settings owing to their simple preparation method and remarkable resistance to corrosion. They have become a primary protective measure for engineering structures [1–3]. Waterborne zinc-rich coatings are particularly popular due to their minimal volatile organic compound emissions and eco-friendly characteristics. Specifically, waterborne epoxy zinc-rich variants not only mitigate environmental pollution when compared to traditional organic coatings, but also exhibit enhanced bonding strength and corrosion resistance in practical use [4–6]. Nevertheless, these waterborne epoxy zinc-rich coatings encounter certain performance issues: (1) A significant quantity of zinc powder is added during the formulation stage, leading to settling and agglomeration of the coatings, which can compromise their effectiveness, necessitating rapid application and thereby presenting hurdles to achieving high-quality and efficient coating application. (2) The coatings are microscopically porous, exhibiting inadequate shielding capabilities. The high concentration of zinc powder in waterborne epoxy coatings

results in insufficient epoxy resin to adequately fill the spaces between the zinc particles, creating a porous structure. In scenarios requiring prolonged immersion in corrosive environments, harmful agents can infiltrate the coating through these pores and reach the substrate beneath the coatings, resulting in protection failure and corrosion damage.

Traditional epoxy zinc-rich coatings typically contain a zinc concentration exceeding 70%. However, as the zinc powder undergoes oxidation, byproducts like zinc oxide can impede the electrical conductive connections between the zinc particles and the formation of micro-galvanic cells, which compromises the coating's cathodic protection for the substrate [7–15]. When the zinc concentration surpasses 80 wt.%, they provide excellent cathodic protection due to the effective electrical conductive connections between the zinc particles; however, this results in a considerable amount of unused zinc powder within the coatings, leading to resource wastage and potential environmental issues. Additionally, elevated zinc concentrations adversely impact the leveling properties, density, adhesion, and flexibility of the coatings [2,16–19]. Orek et al. have performed theoretical and experimental analyses of the electrical, optical, and structural properties of wurtzite (similar to zinc oxide (ZnO)) nanostructures. The effect of quantum constraints on optical properties and two different ZnO clusters in the nanowire structure were investigated [20].

Furthermore, much of the research surrounding zinc-rich coatings has concentrated on the comparison between spherical and flake zinc powders. A large amount of research on zinc-rich coatings focuses on the selection and application of spherical zinc powder or flake zinc powder. Compared with spherical zinc powder, flake zinc powder has a larger specific surface area and higher surface activity, and the prepared zinc-rich coatings have better corrosion resistance. However, flaky zinc powder has some problems, such as poor dispersion and easy corrosion in water-based coating systems [17,21–24].

Numerous studies have identified the incorporation of fillers into zinc-rich coatings as one of the most economical and effective approaches currently available. Innovative conductive fillers such as CNTs and graphene have been utilized by researchers to partially replace zinc powder in the formulation of nano-composite coatings, showing considerable potential for various applications [21,23–27]. CNTs are known for their remarkable conductivity and nanoscale effects. Their incorporation into coatings can reduce internal porosity, lengthen the route for corrosive agents to access the steel substrate, and facilitate electron transfer during the cathodic protection stage. Moreover, CNTs possess electrochemical characteristics. Their potential surpasses that of the metal substrate, which may result in passivation of the metal, thus improving the substrate's corrosion resistance [28–30]. Park et al. utilized a ball milling dispersion method to first disperse multi-walled carbon nanotubes (MWCNTs) in xylene, to develop MWCNT-enhanced epoxy zinc-rich anti-corrosion coatings and explore the effect of MWCNTs on the coatings' performance [4]. Similarly, Wang et al. noted that incorporating CNTs into epoxy coatings with a low zinc concentration improves their ability to resist corrosion. Additionally, incorporating materials such as graphene and graphene oxide into these zinc-rich epoxy coatings significantly improves their ability to resist corrosion [11,16,21,22,31–34].

In summary, the integration of CNTs significantly enhances the electrical conductive connection among zinc particles and the steel substrate compared to zinc-rich coatings, thereby improving protective characteristics of the coatings. This study primarily focuses on a commercially available waterborne epoxy zinc-rich coating, which is Barrier 80 WF (abbreviated as 80 WF) from Jotun company, and enhances it by incorporating multi-walled carbon nanotubes, to improve its corrosion protection for Q355b steel substrate. A thorough array of evaluations were performed, including tests for pencil hardness, adhesion, impact resistance, electrochemical analysis, SEM, EDS, XPS, XRD, and neutral salt spray, to analyze the structure, composition, and corrosion resistance performance of waterborne zinc-rich coatings containing varying amounts of multi-walled carbon nanotubes. Furthermore, the research examined the anti-corrosion mechanisms associated with these CNT-reinforced waterborne epoxy zinc-rich coatings. The results provide

valuable insights for the development of high-performance waterborne epoxy zinc-rich coatings with corrosion protection for Q355b steel substrate.

2. Materials and Methods

2.1. Materials and Preparation of Coatings

The main material utilized was a waterborne coating (80 WF) with a zinc concentration of 70 wt.%, while Q355b steel was chosen as the substrate. Table 1 provides information regarding the chemical composition of Q355b. Following preliminary experiments involving carbon nanotubes and waterborne zinc-rich coatings, multi-walled carbon nanotubes (rolled from multiple layers of graphene) were selected as the filler for modification due to their corrosion resistance and relatively lower cost compared to single-walled carbon nanotubes (rolled from a single layer of graphene). The constituents of the 80 WF utilized in these experiments are outlined in Table 2. To examine how the concentration of multi-walled carbon nanotubes affects the coating's performance, waterborne zinc-rich coatings with different multi-walled carbon nanotube concentration (wt.%) of 0.1, 0.3, 0.5, 0.7, and 1.0 were formulated. The scheme for preparing coatings is depicted in Figure 1. 80 WF is a two-component waterborne epoxy zinc-rich coating cured with polyamine adducts. During the preparation process, components A and B of the commercial 80 WF were firstly combined in a beaker, and then agitated at a speed of 500 r/min to form a thick solution. Afterward, deionized water was added to achieve the desired dilution, and the resulting mixture was stirred at 1000 r/min for a duration of 20 min to guarantee complete dispersion. The uniformly dispersed coating was then applied onto Q355b samples of varying sizes in accordance with different testing standards and cured in an oven at 40 °C for 5 days to create the 80 WF coatings. In a beaker, a mixed solvent with different concentrations of multi-walled carbon nanotubes and dispersants underwent ultrasonic dispersion for 5 min, which was then followed by a low-speed stirring at a rate of 300–500 r/min until homogeneity was reached. Another portion of the previously mentioned uniformly dispersed 80 WF was combined with the multi-walled carbon nanotube solvent and stirred at 500 r/min for 20 min. The coating was subsequently applied to Q355b samples with sizes of 10 mm × 10 mm × 2 mm for electrochemical tests and 50 mm × 50 mm × 3 mm for salt spray tests, and then cured in an oven at 40 °C for a duration of 5 days, leading to the formation of waterborne zinc-rich coatings reinforced with carbon nanotubes (CNTs/80 WF).

Table 1. Chemical composition of Q355b steel.

Element	C	Si	Mn	S	P	Cr	Ni	Cu
wt.%	≤0.24	≤0.55	≤1.60	≤0.035	≤0.035	≤0.24	≤0.30	≤0.30

Table 2. Basic components of 80 WF zinc-rich coating.

Component	Material	wt%
A	Zinc Powder	≥75–≤90
	1-Methoxy-2-Propanol	≤10
	Epoxy Resin (MW 700–1200)	≤5
	Epoxy Resin (MW < 700)	≤4.6
	Zinc Oxide	≤3
	γ-Propyltrimethoxysilane	<3
B	Polyether Polyamine	<25
	1-Methoxy-2-Propanol	≤5
	3-Aminomethyl-3,5,5-Trimethylcyclohexylamine	<2.5
	a,a′-Diaminodimethylbenzene	<2.5
	Sodium Nitrite	≤0.3

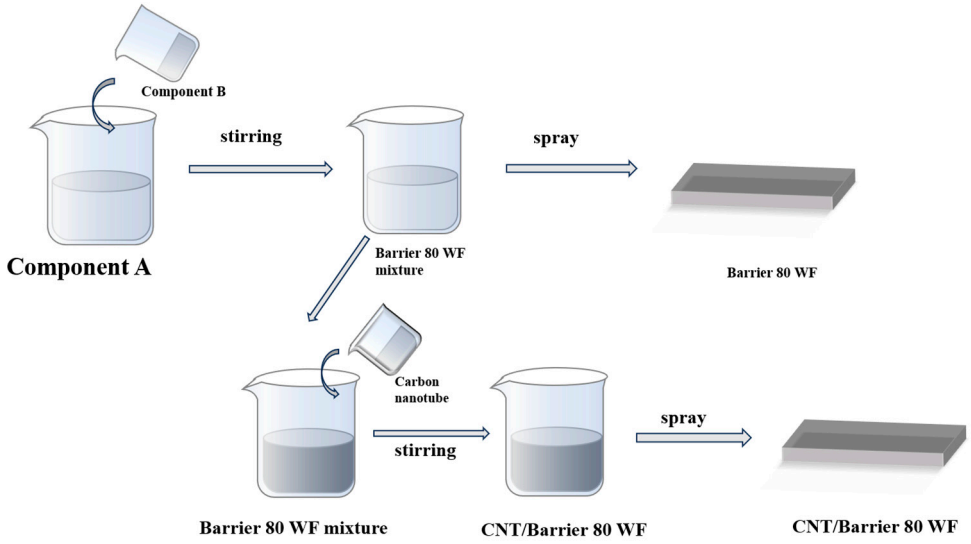

Figure 1. Scheme of preparation of 80 WF and CNTs/80 WF coatings.

2.2. Mechanical Test and Thickness Measurements of Coatings

In accordance with ISO 12944 of "Paints and varnishes-Corrosion protection of steel structures via protective paint systems", various tests for hardness and scratch resistance were carried out on multiple coatings. To assess the thickness of the coatings, an ultrasonic thickness gauge was utilized.

2.3. FTIR Analysis of Coatings

Following the curing of the coatings in an oven at 40 °C for five days, an FTIR test was conducted on the coatings with the Thermo Fisher Scientific Nicolet iS20 instrument (Sydney, NSW, Australia). The samples were prepared utilizing the potassium bromide pellet technique. A strong Globar infrared light source delivered substantial energy. The spectrum's scanning range was set from 4000 cm^{-1} down to 400 cm^{-1}.

2.4. SEM Analysis of Coatings

The morphologies of the sample surface were examined with secondary electron signal imaging by using SEM. This research employed a Sigma 300 SEM (ZEISS, Oberkochen, Germany), operating at a barrel acceleration voltage of 15 kV, achieving a secondary electron image resolution of 0.8 nm. The microscopic structures of the waterborne zinc-rich coatings were analyzed both prior to and following corrosion.

2.5. EDS Analysis of Coatings

In this research, an analysis of different waterborne zinc-rich coatings was performed using the Oxford Ultim Extreme EDS system with SEM capabilities to evaluate the elemental distribution and content both prior to and following corrosion.

2.6. Electrochemical Tests

In this research, various samples of waterborne zinc-rich coatings were immersed in a 3.5 wt.% NaCl solution at approximately 25 °C over a timespan of 28 days. The experimental methods used encompassed open circuit potential (OCP) measurements, electrochemical impedance spectroscopy (EIS), and scanning potentiodynamic polarization (PDP). During the evaluation process, a saturated calomel electrode (SCE) was inserted into the solution and linked to the reference electrode clamp of the electrochemical workstation, while the wire end of the coated sample was connected to the clamp of the working electrode. Once the experiments commenced, EIS and PDP readings were documented once the open circuit potential fluctuations stabilized to below 10 mV. The EIS measurements spanned a frequency range from 10^{-2} to 10^{5} Hz, employing a sine wave signal with an amplitude of

10 mV and collecting data at ten distinct points per decade. Once the tests were conducted, the gathered data were retained, enabling the creation of Nyquist and Bode plots. The impedance data collected were examined with ZSimpWin 3.6 software to understand the corrosion mechanisms involved. To ensure reliable experimental outcomes, three parallel samples of each type of coating were tested.

2.7. Neutral Salt Spray Test

In this study, multiple samples of zinc-rich coatings with size of 50 × 50 × 3 mm underwent a cross-scratching procedure labeled "X". Epoxy resin was used to seal both the edges and the backs of the samples. After the preparation, the samples were placed in a salt spray chamber for the evaluation of neutral salt spray, using a corrosion solution composed of 5 wt.% NaCl and a pH ranging from 6.5 to 7.2. The temperature within the salt spray chamber was maintained at 35 °C, and the air pressure from the pump was controlled to remain between 0.1 and 0.2 MPa. Each set of samples was made up of three parallel specimens, all subjected to uninterrupted spraying for an overall duration of 240 h, during which detailed observations and records of surface changes were carried out.

2.8. XRD Analysis of Coatings

In this study, a Rigaku SmartLab SE XRD instrument (manufactured in Japan, Rigaku Holdings Corporation, Tokyo, Japan) equipped with a copper target was employed, which has a wavelength of 1.5418 Å, operates at a voltage of 40 kV, and a current of 40 mA, while scanning across a range from 5° to 90°. The gathered data were analyzed using Jade 6 software to investigate the changes in the materials located on the surfaces of water-borne zinc-rich coatings, both before and after corrosion.

2.9. XPS Analysis of Coatings

In this study, a device from Thermo Scientific (Sydney, NSW, Australia), namely the K-Alpha XPS (USA), was employed. The X-ray source utilized was a microfocused monochromatic Al Kα source, which allowed for an adjustable spot size between 30 and 400 μm, with a stepping increment of 5 μm. Two scanning methods were executed: a full spectrum scan that spanned an energy range of 100 eV at 1 eV intervals, and a narrow spectrum scan with an energy range of 30 to 50 eV, incrementing by 0.05 to 0.1 eV. To ensure accurate calibration, the reference contaminant C1s (284.8 eV) was used, and the gathered data were analyzed with Avantage 5.9 software to enable peak fitting.

3. Results

3.1. Mechanical Properties of 80 WF Coating and CNTs/80 WF Coatings with Different CNTs Concentration

The test results of the mechanical properties for the coatings are detailed in Table 3. The test of each coating complied with ISO standards regarding flexibility and impact resistance. Initially, as the concentration of CNTs increases, both the hardness and bonding strength of the coatings improve, but they eventually start to decrease. A maximum pencil hardness of 4 H was obtained at a CNTs concentration of 0.3 wt.%, significantly exceeding the national standard of 3 H. This enhancement is largely due to the intrinsic hardness of the CNTs, which elevates the overall hardness of the coating. On the other hand, an overly high concentration of CNTs can lead to agglomeration within the coating, which may decrease hardness, especially in the coating with 1.0 wt.% CNTs. Furthermore, due to the nanoscale properties of CNTs, these materials can efficiently fill the gaps created by steric hindrance between zinc powder and epoxy resin, thus improving the adhesion between layers. However, if the CNT concentration surpasses a specific limit, the agglomeration of these nanoparticles may create localized stress concentrations within the coating, ultimately leading to a decrease in hardness.

Table 3. Mechanical properties of coatings.

Coating Test Items	Coating Type					
	80 WF	0.1 wt.%	0.3 wt.%	0.5 wt.%	0.7 wt.%	1.0 wt.%
Pencil hardness test	2 H	3 H	4 H	3 H	3 H	2 H
Impact testing of coatings (cm)	50	50	50	50	50	50

3.2. FTIR Analysis of 80 WF Coating and CNTs/80 WF Coating

The Fourier transform infrared spectra of the 80 WF and CNTs/80 WF coatings are depicted in Figure 2. The peaks observed at 3426 cm^{-1} are generally linked to the stretching vibration of O-H bonds, potentially originating from hydroxyl groups in water or polyether polyamines. At 2928 cm^{-1}, the spectra reveal a stretching vibration of the C-H bond, particularly linked to both methyl and methylene groups. The peaks observed at 1609 cm^{-1} could denote the C=C stretching vibration, which is commonly found in unsaturated compounds, including the principal monomers used in epoxy resins. At 1506 cm^{-1}, the peaks might indicate C=C stretching vibrations occurring in aromatic rings, which may originate from the fundamental structure of the epoxy resin or compounds such as a,a′-diaminodimethylbenzene. Furthermore, the peaks situated at 1240 cm^{-1} are generally attributed to C-N stretching vibrations, likely arising from amines like polyether polyamines or aminomethyl substances such as 3-amino-3,5,5-trimethylcyclohexylamine. The peaks found at 1183 cm^{-1} and 1098 cm^{-1} may be associated with C-O-C bond stretching vibrations presented in epoxy resins as well as in 1-methoxy-2-propanol. The peaks at 827 cm^{-1} probably correspond to C-H bending vibrations from ring structures or distinctive vibrations attributed to certain substituents, particularly within the frameworks of aromatic rings. Lastly, the peaks at 550 cm^{-1} in the lower wavenumber region signifies Zn-O stretching vibrations. The FTIR spectra for both coatings reveal that incorporating CNTs does not lead to considerable alterations in the peak positions, although some peak areas for the CNTs/80 WF coating appear reduced. These findings imply that the modification of the coatings with CNTs is mainly a physical doping process, and the carbon nanotubes do not react chemically with the components of the coating.

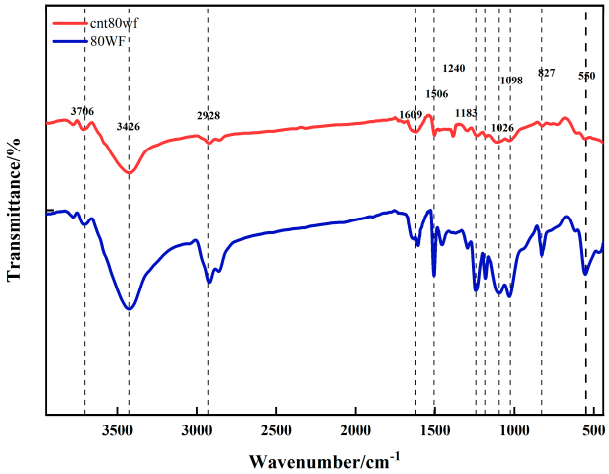

Figure 2. Fourier transform infrared spectra of 80 WF and CNTs/80 WF coatings.

3.3. Surface Morphologies and EDS Analysis of 80 WF Coating and CNTs/80 WF Coatings

An SEM image of the original multi-walled carbon nanotubes is shown in Figure 3. Figures 4–6 depict the surface morphologies and EDS spectra of coatings without CNTs (80 WF), with 0.3 wt.% CNTs and 1.0 wt.% CNTs, respectively. In Figure 4, it is evident that the coating's surface comprises a considerable quantity of spherical zinc particles. The film-forming agents, such as epoxy resin, are capable of adequately encapsulating

the zinc particles; however, the coating's surface exhibits irregularities, with the spherical zinc particles distributed unevenly. The zinc particle is isolated and cannot be well connected, and the overall coating is not too dense. Conversely, Figure 5 demonstrates that the incorporation of CNTs leads to their stable adhesion to the coating surface, thereby enhancing the coating's density. This implies that the CNTs occupy the gaps between the zinc particles and epoxy resin, contributing to a shielding effect. The morphology of the surface suggests that the CNTs form connections with the zinc particles, thereby creating a conductive path between neighboring spherical zinc particles. However, as illustrated in Figure 6, a rise in the CNT content results in a markedly uneven distribution and clustering of CNTs on the coating surface containing 1.0 wt.% CNTs, potentially compromising the coating's properties and its resistance to corrosion. Surface analyses conducted using EDS on all three coatings reveal that the concentrations of Zn, C, and O elements are relatively elevated, with these elements uniformly distributed across the coating's surface.

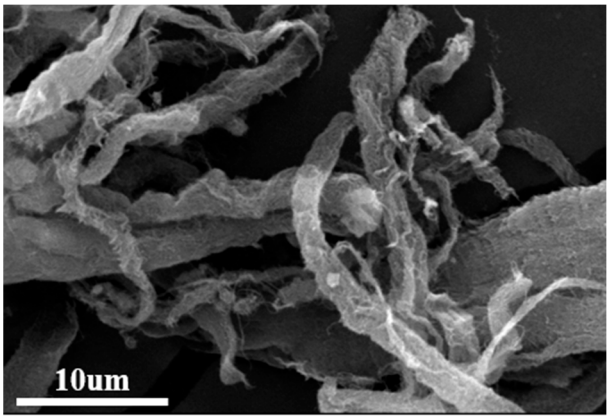

Figure 3. SEM image of the original CNTs.

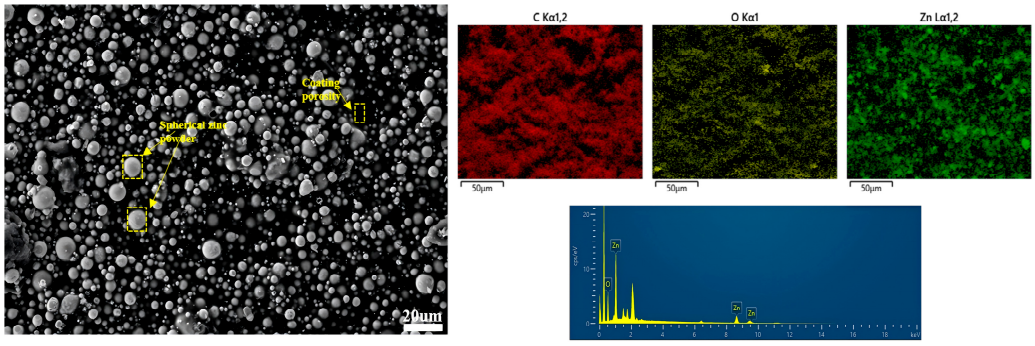

Figure 4. SEM and EDS of 80 WF.

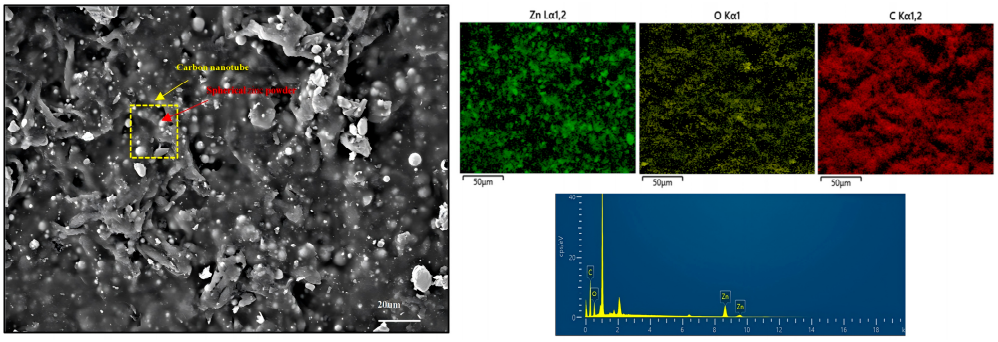

Figure 5. SEM and EDS of 0.3 wt.% CNTs/80 WF.

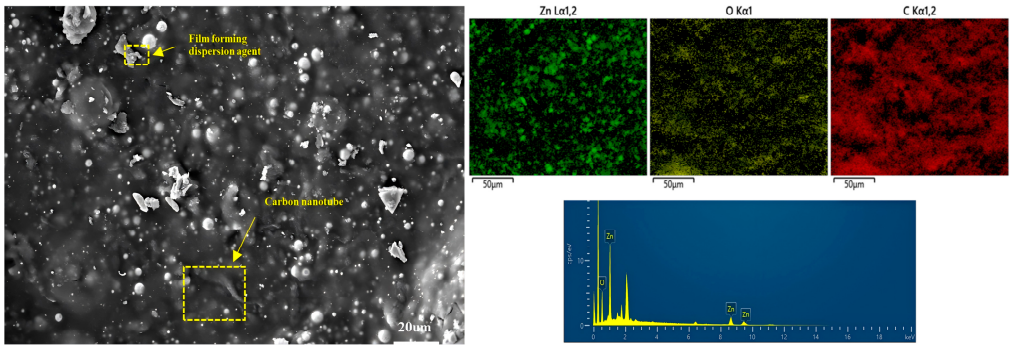

Figure 6. SEM and EDS of 1.0 wt.% CNTs/80 WF.

3.4. OCP, EIS, and PDP Tests of 80 WF Coating and CNTs/80 WF Coatings with Different CNTs Concentration

The 80 WF coating and coatings with five different concentrations of CNTs were subjected to electrochemical testing at different time intervals after immersion. The performance of coatings rich in zinc for cathodic protection is typically assessed by measuring their OCP. When the OCP drops below −0.78 V, it signifies that the coating still possesses a considerable ability to provide cathodic protection to steel substrate. In contrast, an increase in the OCP beyond −0.78 V signifies a decline in the coating's ability to offer cathodic protection, indicating a transition towards a shielding protection phase. Figure 7 demonstrates that with an increase in immersion time, each coating exhibits a gradual rise in OCP. The figure clearly shows that the coating without CNTs (80 WF) and the coating incorporating 0.1 wt.% CNTs offer minimal to no cathodic protection, as indicated by their OCP values staying above −0.78 V. In contrast, the 0.3 wt.% CNTs coating maintains cathodic protection for the maximum duration of 14 days. Nevertheless, a rise in the CNTs concentration results in a shortened period of cathodic protection. A moderate quantity of CNTs improves the conductive connections among zinc particles and the steel substrate, thereby promoting the formation of a strong electrical conductive pathway. Consequently, this improves the efficiency of cathodic protection and increases the corrosion resistance of the coating. Conversely, an overabundance of CNTs leads to a decreased lifespan of cathodic protection, primarily due to the swift removal of spherical zinc particles from the surface of the coating.

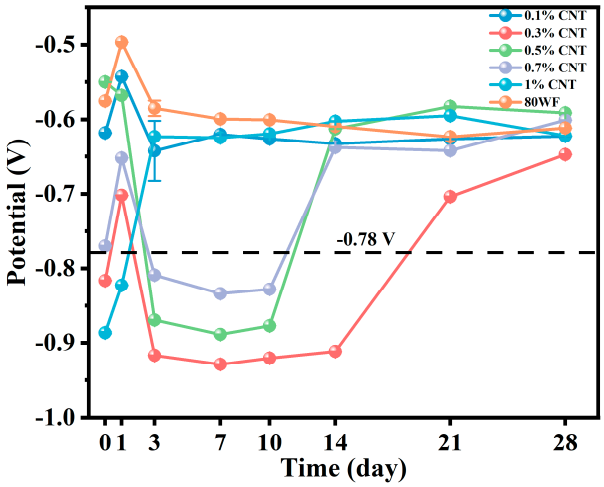

Figure 7. Open circuit potential (OCP) curves of 80 WF and waterborne zinc-rich coatings with 0.1 wt.%–1 wt.% CNTs after 28 days of immersion.

The electrochemical impedance spectra (EIS) of the coatings are presented in Figures 8 and 9. These spectra have been analyzed and fitted using the equivalent circuit shown in Figure 10.

Within this circuit, R_s represents the resistance of the corrosion electrolyte. Furthermore, R_c indicates the resistance of the coating that is applied to the surface. Rather than utilizing a traditional capacitance for the coating, a Constant Phase Element (CPE) is used to more effectively represent the non-ideal behavior in the system, and R_{ct} denotes the charge transfer resistance. Additionally, Warburg impedance is utilized to correct errors associated with diffusion behavior. Examination of the Nyquist plots presented in Figure 8(a1–c1) indicates that the CNTs/80 WF coatings, apart from the 1.0 wt.% CNTs coating, exhibit a larger initial capacitive arc radius in comparison to the unmodified 80 WF coating. Among the six coatings, the coating with 0.3 wt.% CNTs consistently exhibits a larger capacitive arc radius compared to the other five coatings during the same immersion period [34]. Moreover, an increase in the concentration of CNTs from 0.5 wt.% to 1.0 wt.% is associated with a decrease in the capacitive arc radius. As illustrated in Figure 11, the R_{ct} values of the coatings initially rise before experiencing a decrease. The coating incorporated with 0.3 wt.% CNTs exhibits the highest R_{ct} value of 3756, suggesting that its resistance to corrosion is superior to that of the other five coatings. The impedance modulus of the coating with 0.3 wt.% CNTs is observed to be significant at low frequencies. This finding indicates that the coating with 0.3 wt.% CNTs exhibits superior corrosion resistance when compared to the other coatings analyzed in the study. This enhanced performance suggests that incorporating this specific concentration of CNTs into a coating formulation may effectively improve its protective efficiency against corrosion, thereby potentially increasing the longevity and durability of materials subjected to corrosive environments.

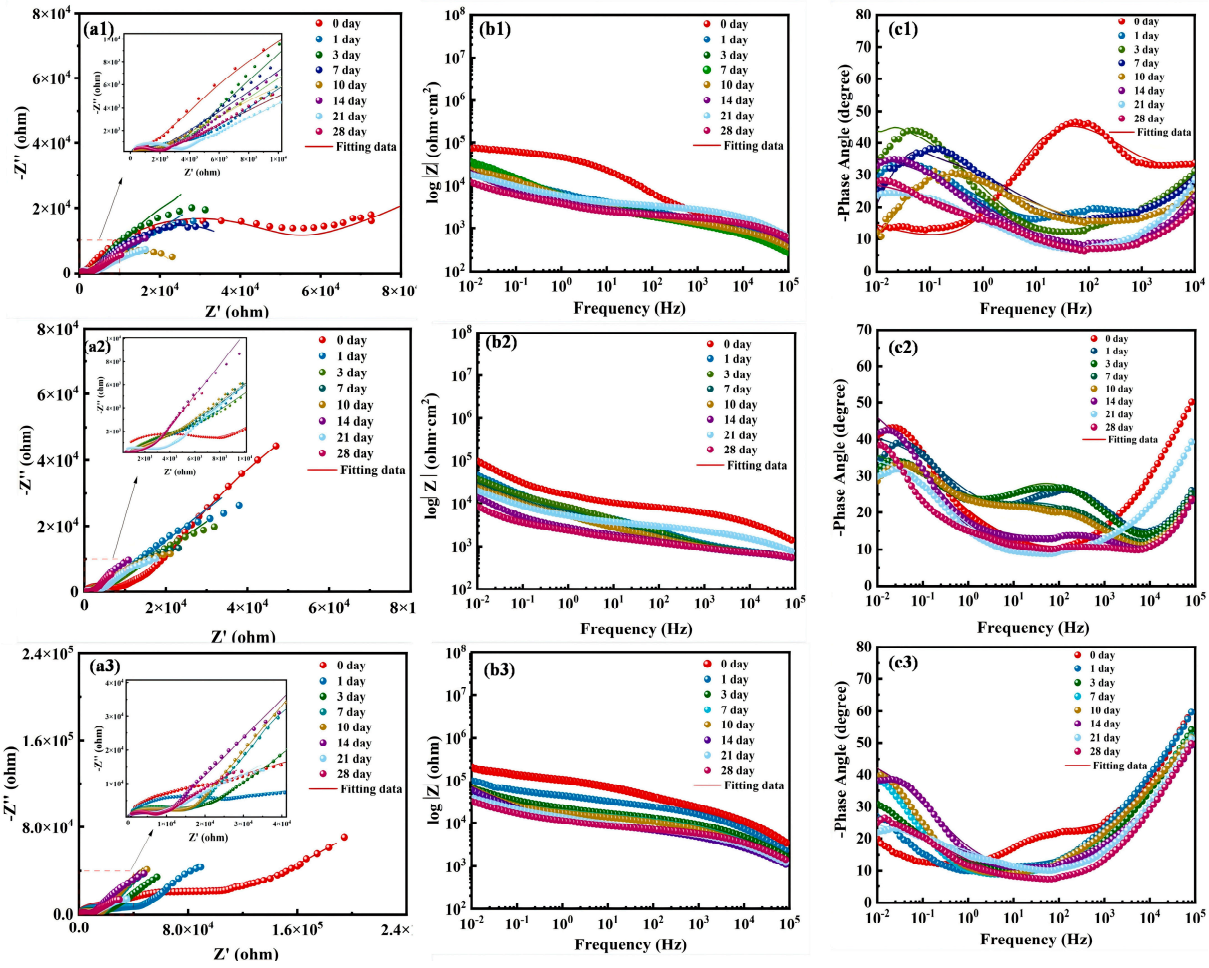

Figure 8. Nyquist plot and Bode plot of electrochemical impedance spectroscopy (EIS) for the 80 WF coating and waterborne zinc-rich coatings with varying CNT content after 28 days of immersion: (**a1–c1**) representing 80 WF, (**a2–c2**) indicating 0.1 wt.% CNTs, and (**a3–c3**) showing 0.3 wt.% CNTs.

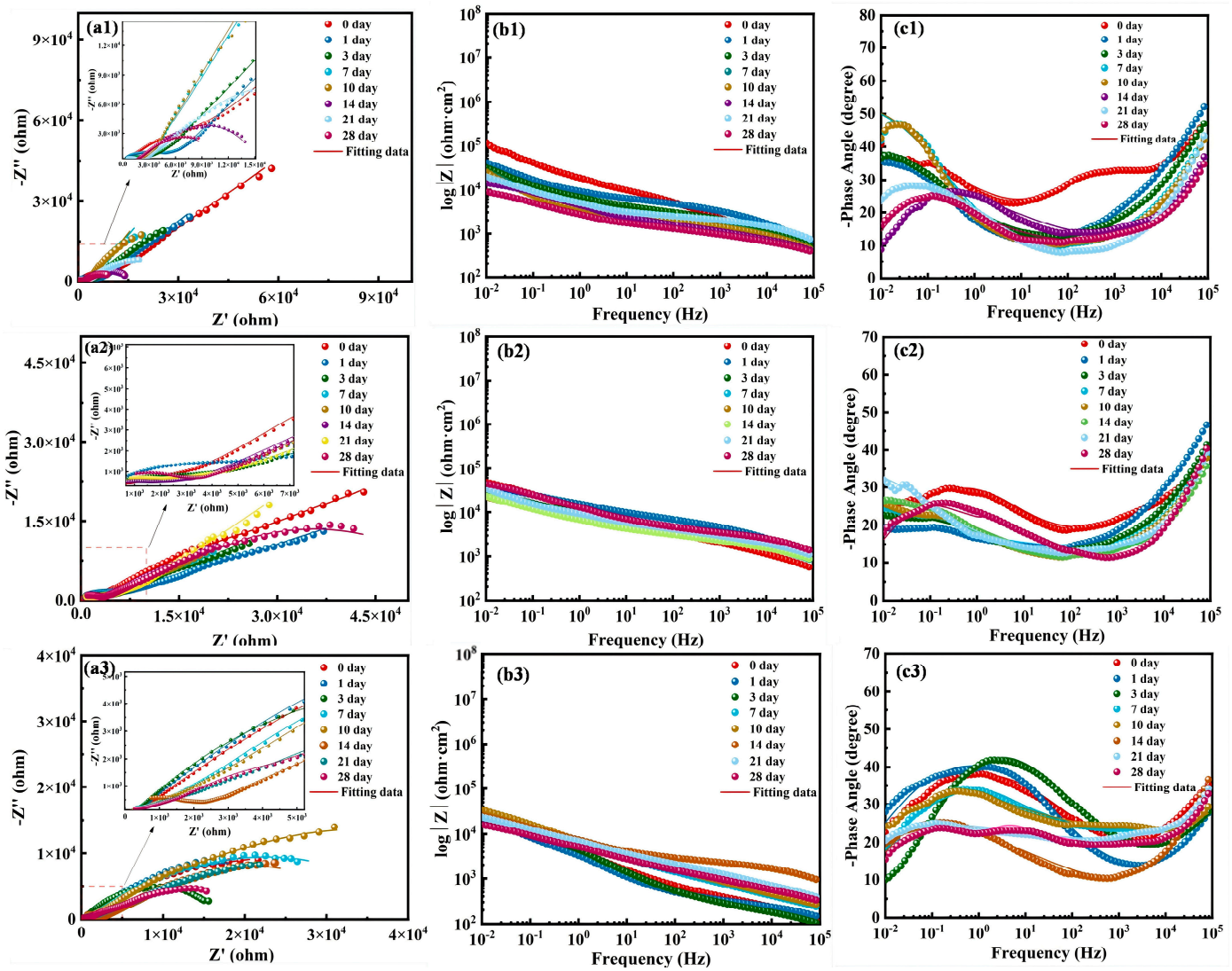

Figure 9. Nyquist plot and Bode plot of EIS for zinc-rich coatings dispersed in water, containing varying amounts of CNTs, examined after 28-day immersion: (**a1**–**c1**) with 0.5 wt.% CNTs, (**a2**–**c2**) containing 0.7 wt.% CNTs, and (**a3**–**c3**) featuring 1.0 wt.% CNTs.

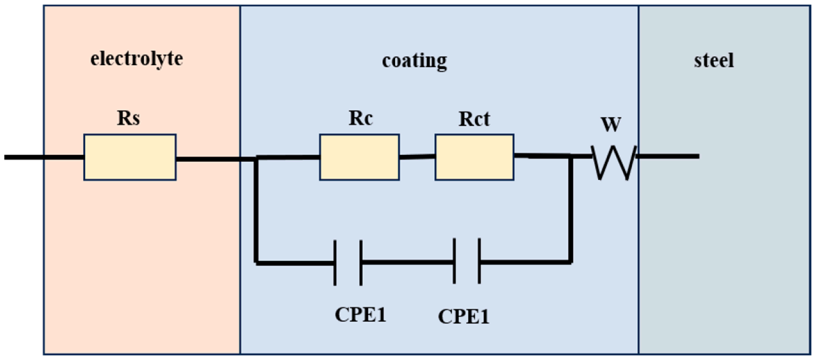

Figure 10. Equivalent circuit diagram for EIS fitting of immersed coatings.

All six coatings demonstrate a notable shift towards higher frequency values with prolonged immersion time, suggesting a decline in their effectiveness of physical protection. This shift represents a transition from sufficient physical protection to potential failure. In addition, trends analogous to those observed in the previous EIS results are present among

the six coatings, highlighting that the diffusion of corrosive media in the coating containing 0.3 wt.% CNTs is restricted. This additionally supports the idea that the coating with 0.3 wt.% CNTs provides improved physical shielding capabilities and greater corrosion resistance in comparison to the other formulations [7,35–39].

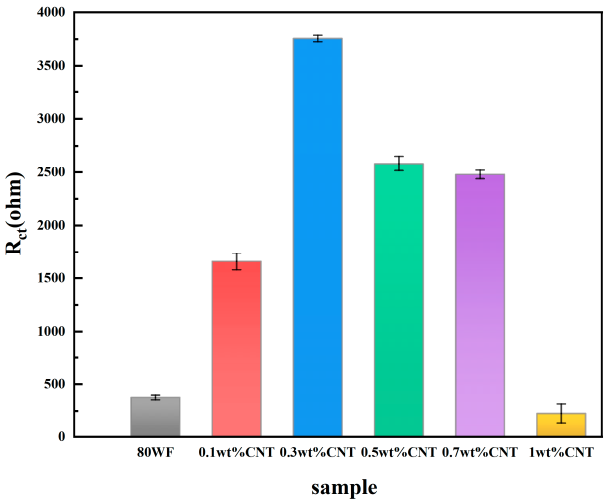

Figure 11. The fitted Rct values for different coatings after 28 days of immersion.

Specifically, a lower self-corrosion current density is indicative of a decreased rate of corrosion, suggesting enhanced corrosion resistance. The findings regarding various coatings after an immersion duration of 28 days are visually represented in Figure 12, which displays the polarization curves corresponding to each coating. The detailed parameters, including corrosion potential (E_{corr}), corrosion current density (i_{corr}), anodic Tafel slope (β_a), and cathodic Tafel slope (β_c) associated with these curves can be found in Table 4. The data presented in the figure reveal that the self-corrosion current density for coatings modified with different concentrations of CNTs initially increases before subsequently decreasing. Table 4 provides the specific parameters associated with these curves. The information depicted in this figure suggests that the self-corrosion current density for coatings modified with different concentrations of CNTs initially increases and then ultimately decreases. Notably, when a concentration of 0.3 wt.% of CNTs is added, the resultant coating demonstrates the lowest self-corrosion current density of 0.0322 μA/cm^2. This finding indicates that this particular composition offers the most effective corrosion resistance, establishing an optimal balance in the application of CNTs for improving coating performance.

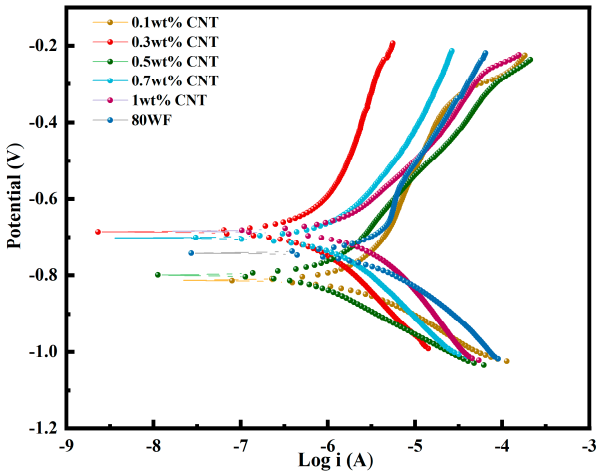

Figure 12. Tafel plots were generated for zinc-rich coatings and 80 WF, incorporating various contents of CNTs (0.1 wt.%–1.0 wt.%) following 28-day immersion.

Table 4. The relevant parameters of the Tafel plots for 80 WF and zinc-rich coatings with different CNT contents.

CNT Concentration (wt.%)	0.1	0.3	0.5	0.7	1.0	0
Corrosion potential E_{corr} (v)	−0.813	−0.685	−0.799	−0.702	−0.684	−0.743
Corrosion current density I_{corr} (A/cm^2)	0.086	0.032	0.054	0.070	0.084	0.155
Anodic Tafel slope β_α	8.090	5.520	5.530	5.170	7.580	7.370
Cathodic Tafel slope β_c	13.570	7.540	7.120	6.520	9.540	10.580

The primary explanation for the previously discussed outcomes could be associated with the ability of the epoxy resin to absorb moisture, leading to its expansion. The expansion, in turn, obstructs the penetration of harmful substances, serving as an effective barrier against the entry of solution. As the immersion period is extended, the zinc-rich coating engages with corrosive substances, allowing zinc particles to provide cathodic protection for the underlying Q355b steel substrate. This engagement generates corrosion byproducts that can physically limit harmful agents from reaching the Q355b steel substrate.

CNTs exhibit remarkable electrical conductivity and possess nanoscale properties. Incorporating CNTs into the 80 WF coating significantly decreases the shrinkage rate during the curing process of the coating, which consequently reduces the formation of micro-pores and effectively seals any pores that were already present. This process slows the infiltration of water and conductive ions within the coating, extending the distance that the corrosive media must travel to reach the Q355b steel substrate. Furthermore, the evenly distributed CNTs can act as electrical conductive pathways in the coating, connecting the spherical zinc particles, which promotes electron transfer during the cathodic protection phase. As the CNTs interconnect the isolated zinc particles, the efficiency of activated zinc powder utilization is improved, resulting in the development of denser or thicker zinc-rich corrosion products within the 0.3 wt.% CNTs coating. This enhances cathodic protection for the Q355b steel and improves the coating's corrosion resistance. During a prolonged immersion duration, the Bode plots indicate a steady decrease in the impedance values, implying either an increase in the size or the quantity of pores that enhance the movement of the corrosive electrolyte. This trend accelerates the corrosion rate at the interface and may prompt the formation of new diffusion layers. Potential degradation of the coating may ensue, leading to a gradual diminishment of its protective performance.

As the quantity of CNTs incorporated into the coating rises, issues such as uneven dispersion and agglomeration of CNTs may arise, which can reduce the coating's performance. Additionally, increased local concentrations of CNTs can elevate the conductivity in these agglomerated regions, leading to a more rapid reaction of the zinc powder at these sites. As a result, the duration of physical shielding offered by zinc corrosion products might be reduced, which could adversely affect the coating's resistance to corrosion. For example, coatings incorporating 0.7 wt.% and 1.0 wt.% CNTs show that a high concentration of CNTs on their surfaces initiates a swift reaction with zinc powder, resulting in a reduced overall protective lifespan of the coating. Furthermore, a considerable amount of CNTs could result in notable interactions between the steel substrate and the CNTs. A significant corrosion current may develop on the coating's surface, which can lead to severe galvanic corrosion that potentially accelerates the degradation of the steel substrate and compromises the cathodic protection provided by the coating. This effect is supported by the observation of surface protrusions on the 1.0 wt.% CNTs coating after undergoing electrochemical testing, demonstrating that an excess of CNT concentration promotes galvanic corrosion

with the Q355b steel substrate, contributing to internal rust formation within the substrate, ultimately diminishing its protective qualities.

3.5. Neutral Salt Spray Test of 80 WF Coating and CNTs/80 WF Coatings with Different Carbon Nanotube Concentrations

After conducting a 240 h evaluation with salt spray test, the results regarding the conventional 80 WF coating and the CNTs/80 WF coatings with different CNTs concentration are illustrated in Figure 13. The data indicate that following the 240 h salt spray test, the 80 WF-coated specimen exhibits some blistering, although there is no significant color change. However, substantial rust is observed in the scratched areas, with corrosion products extending laterally and the corrosion depth at the scratch surpassing 1 mm. For the CNTs/80 WF coatings, a higher CNTs concentration correlates with a gradual increase in the coatings' resistance to salt spray. In particular, for the coating with 0.3 wt.% CNTs, the development of white zinc corrosion byproducts progresses slowly on the surface, while minimal rust appears in the scratched regions. This finding implies that the coating maintains a certain level of protective capability and exhibits commendable corrosion resistance. Conversely, when the CNT concentration is raised, a rapid emergence of white zinc on the surface of the 1.0 wt.% CNTs/80 WF coating is noted, leading to considerable corrosion of the underlying substrate. An excess of CNTs suggests a rapid reduction in zinc levels, thereby diminishing the efficacy of cathodic protection. Furthermore, the aggregation of numerous CNTs may adversely affect the crucial properties of 80 WF, potentially accelerating the corrosion of the steel substrate. To summarize, an optimal concentration of CNTs in the coating not only serves as a protective filler but also creates a bridging pathway between zinc particles, thereby enhancing the reactivity and efficient use of zinc.

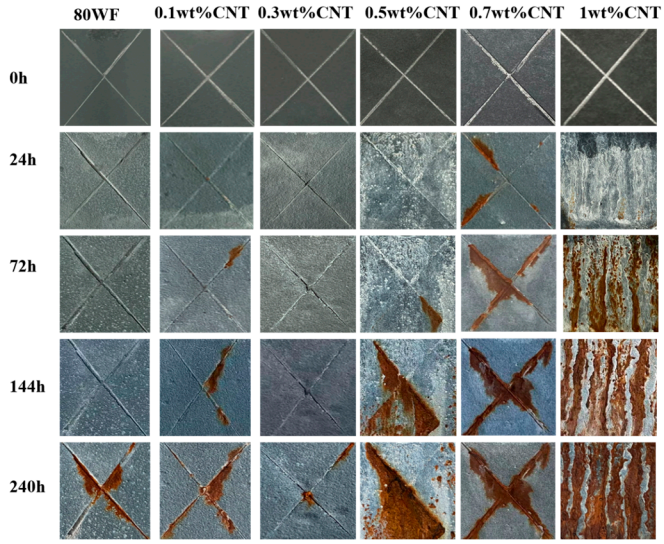

Figure 13. Samples of 80 WF coating and CNTs/80 WF zinc-rich coatings with different CNT contents after 240 h of salt spray test.

3.6. Surface Morphologies and Elemental Changes of 80 WF Coating and CNTs/80 WF Coatings After Corrosion

Figures 14–16 display SEM images and EDS spectra that demonstrate the surfaces of traditional 80 WF coatings as well as those incorporated with 0.3 wt.% and 1.0 wt.% CNTs after immersion. The visuals indicate that after immersion, the surface of the 80 WF coating displayed irregular features. The clustering of zinc powder alongside corrosion byproducts is distinctly observable, alongside a rise in pore dimensions and a reduction in coating density. In Figure 15, the surface morphology of the coating with 0.3 wt.% CNTs post-immersion is shown, highlighting a layered structure of flaky corrosion products on the coating. This layer provides a relatively dense layer across the surface. The EDS

analysis conducted in this region indicates that the flaky corrosion byproducts primarily comprise zinc corrosion compounds, including ZnO, $Zn(OH)_2$, and $Zn_5(OH)_8Cl_2$, along with unreacted zinc powder. Furthermore, almost no Fe can be found on the coating surface, suggesting that the substrate stays uncorroded and the coating provides significant protection. The findings indicate that adding CNTs enhanced the conductive connection between the spherical zinc particles and the Q355b steel substrate, thereby creating a continuous conductive pathway among the zinc powder. This enhancement results in the more effective use of zinc and supports the formation of zinc corrosion byproducts. The flaky products produced through corrosion fill the pores in the coating, hindering the penetration of corrosive agents to the substrate. As a result, this improves the effectiveness of cathodic protection along with the coating's barrier properties, leading to a significant enhancement in its resistance to corrosion.

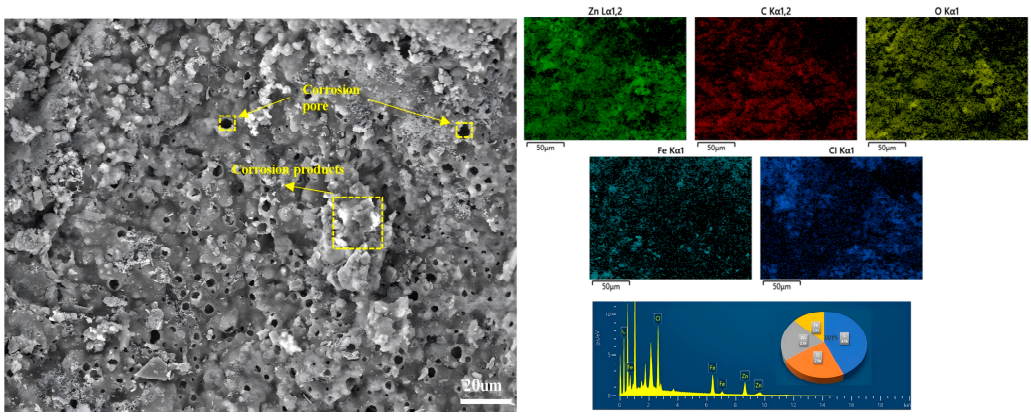

Figure 14. Images from SEM and EDS of the 80 WF coating following a 28-day immersion.

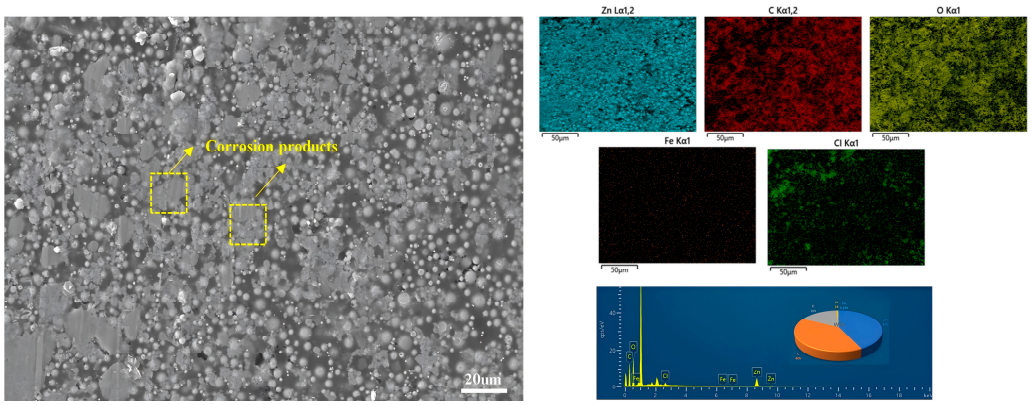

Figure 15. Images from SEM and EDS of the 0.3 wt.% CNTs coating following a 28-day immersion.

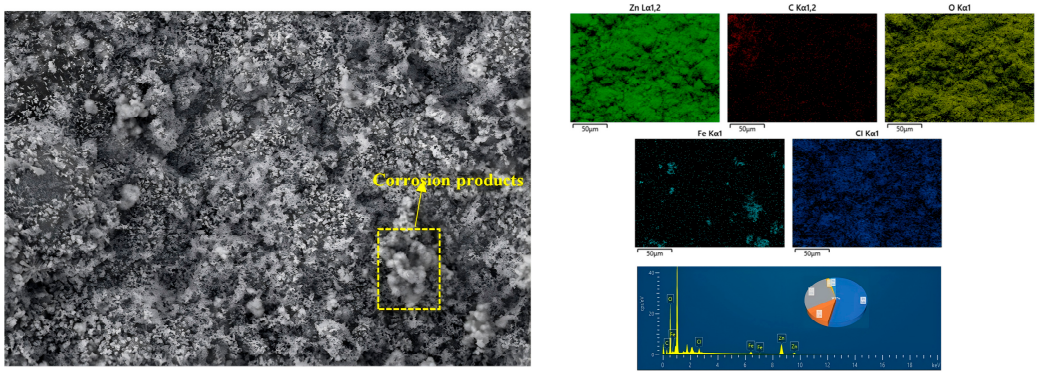

Figure 16. Images from SEM and EDS of the 1 wt.% CNTs coating following a 28-day immersion.

Concerning the coating with 1.0 wt.% CNTs, Figure 16 depicts a significant amount of zinc corrosion products that appear to be unevenly spread across the coating's surface. This phenomenon's emergence is linked to increased concentration of CNTs, which may result in galvanic corrosion between the CNTs and the Q355b steel substrate beneath, consequently accelerating the substrate's corrosion rate. Moreover, the clustering of CNTs causes a swift exhaustion of the nearby zinc powder, and results in corrosion products forming into loose, needle-like structures instead of flaky varieties. The diminished density of the coating enables corrosive substances to infiltrate the coating to reach the substrate, leading to the corrosion of the steel. Analysis of the energy spectrum indicates that corrosion products of iron formed on the coating's surface, suggesting that the substrate is starting to corrode. The effectiveness of the coating as a protective barrier is compromised, resulting in reduced corrosion resistance.

3.7. XRD and XPS Analysis of 80 WF Coating and CNTs/80 WF Coatings After Corrosion

Figure 17 displays the XRD patterns of the coating's surface following 240 h of immersion. The findings reveal that the main corrosion product found in the composite coating is $Zn_5(OH)_8Cl_2$. After the 240 h immersion, a significant reduction in zinc content is observed in the 1.0 wt.% CNTs coating, along with a rise in the intensity of the Fe diffraction peaks. At this stage, the coating ceases to deliver cathodic protection for the underlying material. Conversely, the coating containing 0.3 wt.% CNTs maintains a significant amount of unreacted zinc on its exterior after immersion, with the Fe diffraction peaks showing only a modest intensity. The findings indicate that a coating containing 0.3 wt.% CNTs continues to provide cathodic protection to the substrate. This is evident as corrosion byproducts, such as $Zn_5(OH)_8Cl_2$, efficiently cover the coating's surface and fill the pores. This mechanism successfully separates the substrate from the corrosive environment, improving the coating's physical barrier characteristics. It should be noted that the intensity of the corrosion byproduct, $Zn_5(OH)_8Cl_2$, appears to remain relatively constant despite changes in CNT concentration. This suggests that the corrosion process is affected by CNT concentration, but the formation of $Zn_5(OH)_8Cl_2$ is not significantly altered under the studied conditions.

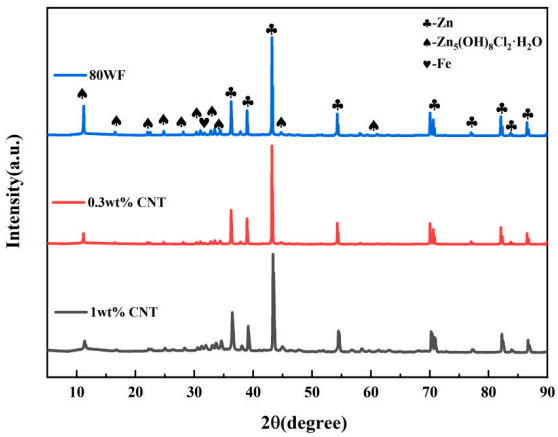

Figure 17. The XRD patterns for zinc-rich coatings containing 80 WF, 0.3 wt.% CNTs, and 1.0 wt.% CNTs following a 240 h immersion.

Figure 18 displays the full XPS spectra of the coatings' surfaces following 240 h of immersion. When compared to the coating with 0.3 wt.% CNTs, the intensity of the Zn2p peak at the binding energy appears to be less prominent for both the 80 WF coating and the 1.0 wt.% CNTs coating. This observation indicates that following corrosion, the zinc on the surfaces of the former two coatings is nearly depleted, while corrosion products originating from the steel substrate accumulate on the coating surface, ultimately leading to its failure. In contrast, the Zn2p peak in the coating with 0.3 wt.% CNTs is distinctly prominent, and

no clearly detectable Fe2p peak can be found. This implies that the 0.3 wt.% CNTs coating remains largely preserved on the steel substrate's surface, with a substantial amount of unreacted zinc powder still present there.

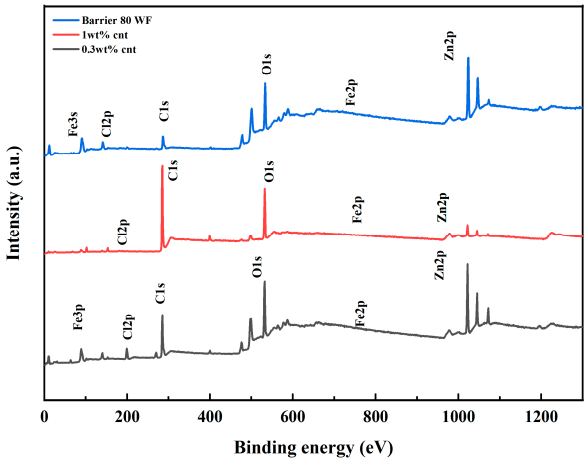

Figure 18. The complete XPS spectra of zinc-rich coatings containing 80 WF, 0.3 wt.% CNTs, and 1.0 wt.% CNTs were obtained following a 240 h immersion.

Figures 19–21 present the XPS fine spectra for the elements Zn, Cl, C, and O in the coatings after 240 h of immersion. The spectral profiles of the elements of all three coatings exhibit significant similarities. In Figure 19a, the presence of the Zn element is predominantly observed as a single compound. A notable peak appears at a binding energy of 1023.1 eV, probably linked to the creation of $Zn(OH)_2$ resulting from the interaction between the zinc powder and OH^- ions in the corrosive environment. Figure 19d reveals three distinct peaks for the O element at varying binding energies. The peak observed at 530.9 eV likely signifies ZnO, which might arise from the decomposition of $Zn(OH)_2$. Furthermore, the peak observed at 532.6 eV is associated with $ZnCO_3$, potentially resulting from the interaction of $Zn(OH)_2$ with CO_2 from the atmosphere. In contrast, the peak at 531.1 eV for $Zn_5(OH)_8Cl_2$ signifies one of the ultimate corrosion products formed from the zinc-rich coating in chloride solutions, generated through the reaction of $Zn(OH)_2$ with $ZnCl_2$.

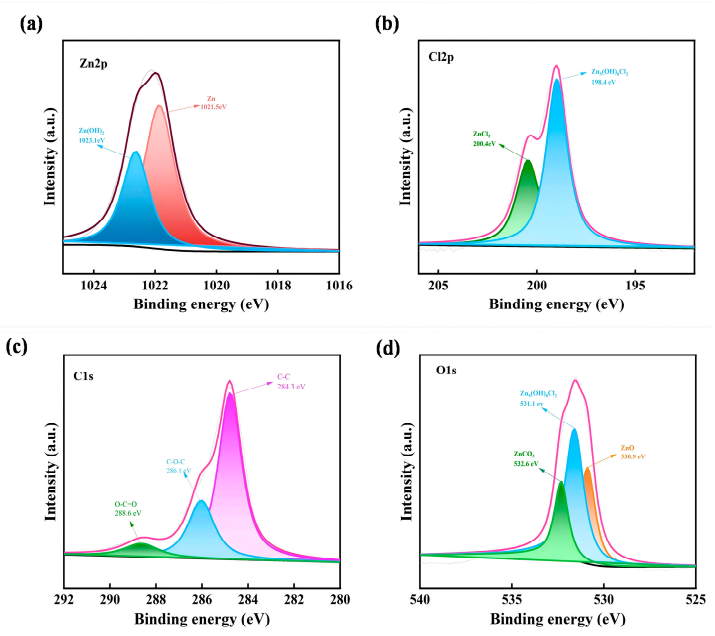

Figure 19. The fine XPS spectra of the 80 WF coating following 240 h of immersion. Fine spectra for the elements (**a**) Zn, (**b**) Cl, (**c**) C, and (**d**) O.

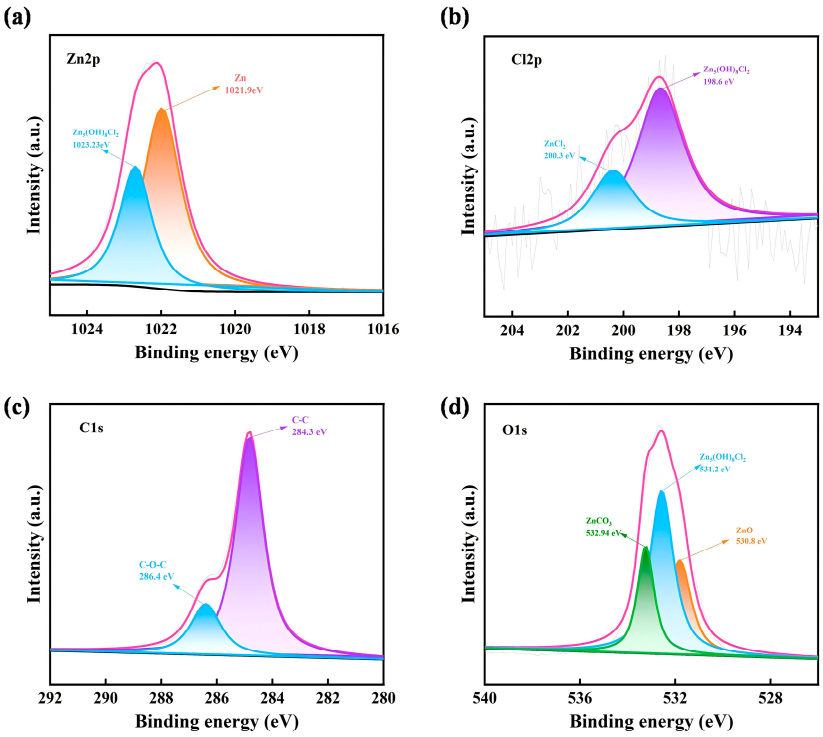

Figure 20. The fine XPS spectra of the 0.3 wt.% CNTs coating following immersion. of immersion. Fine spectra for the elements (**a**) Zn, (**b**) Cl, (**c**) C, and (**d**) O.

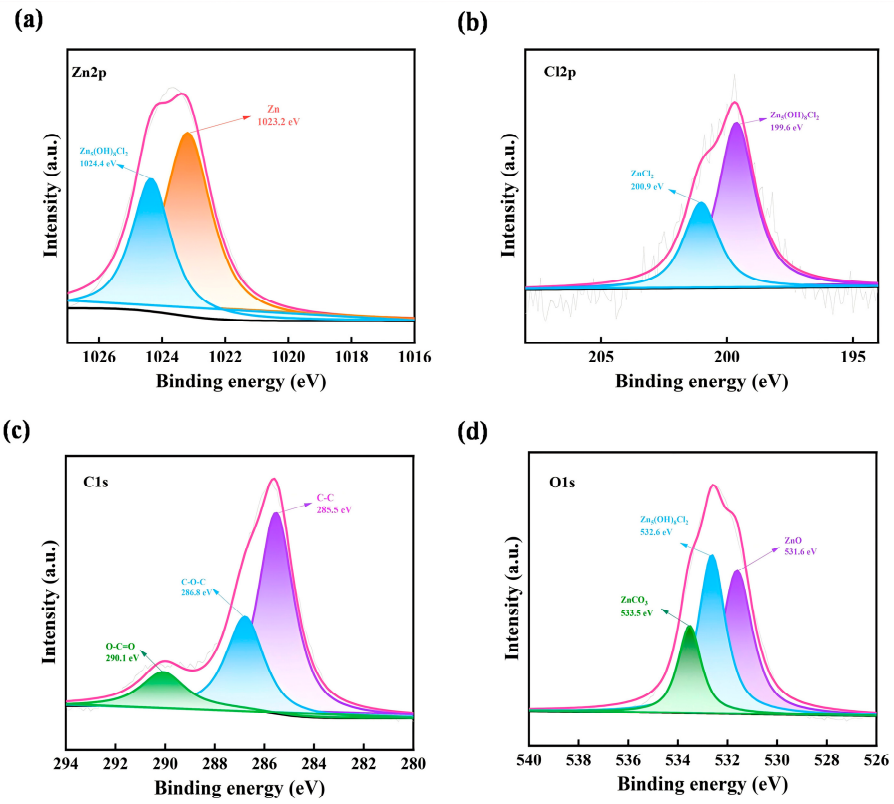

Figure 21. The fine XPS spectra of the 1 wt.% CNTs coating following immersion. Fine spectra for the elements (**a**) Zn, (**b**) Cl, (**c**) C, and (**d**) O.

3.8. The Corrosion Resistance Mechanism of the Coatings

Figure 22 depicts the mechanism of the corrosion reaction, while Figure 22a,b illustrate the processes related to the 80 WF coating without CNTs and the CNTs/80 WF coating after corrosion, respectively. Initially, during the corrosion process, a protective layer is provided by epoxy resin, which shields against corrosive agents such as H_2O, O_2, and Cl^- present in the electrolyte. The epoxy resin protective layer inhibits the infiltration of these substances in the electrolyte into the coating by a physical barrier effect, preventing corrosive agents from reaching the Q355b steel substrate beneath the coating, thereby averting the subsequent corrosion of the Q355b steel substrate. Nonetheless, the formation of micropores on the surface of the coatings is inevitable, and as the immersion duration extends, these corrosive substances begin to permeate through the micropores. In situations where the 80 WF coating does not contain CNTs, the capacity of zinc powder to offer cathodic protection is limited, resulting in the development of zinc corrosion products solely in certain localized areas. The locally generated zinc corrosion products result in an insufficient density within the coating, which cannot effectively prevent corrosive agents from penetrating further, ultimately reaching the Q355b steel substrate and resulting in corrosion. By incorporating CNTs, this issue is alleviated as they fill the pores within the coating and extend the route for corrosive agents to engage with the Q355b steel substrate. This enhancement improves the coating's density and its physical protective characteristics, consequently increasing the longevity of the coating [40,41].

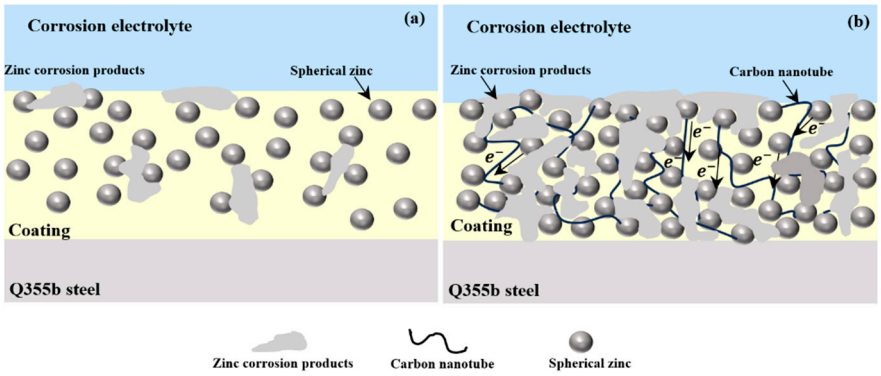

Figure 22. Corrosion resistance diagrams of the coatings: (**a**) the corrosion process associated with the 80 WF coating; (**b**) the corrosion process related to the CNTs/80 WF coating.

Additionally, corrosive agents consistently penetrate, creating microcurrent zones within the particles of zinc powder and in the spaces between these particles and the underlying substrate. The standard electrode potential of zinc powder (−0.78 V) is less than that of Q355b steel, causing the zinc powder to act as the anode and discharge electrons in these microcurrent regions. Consequently, the zinc powder particles corrode first, which helps to protect the steel substrate, acting as the cathode. The uniformly distributed CNTs improve the electrical conductive connections among isolated zinc particles, leading to many more active zinc particles for the cathodic protection of Q355b steel substrate. An increased number of zinc particles further enlarges the specific surface area for both the anode and cathode, subsequently enhancing zinc dissolution and facilitating sustained cathodic protection for the coating [16,20,22,25,35].

When the coating and the substrate are corroded directly, as the anode, the zinc powder corrodes preferentially and plays a role of cathodic protection as the sacrificial anode. This procedure entails a reaction between O_2 in the ambient air and H_2O within the corrosion medium, leading to the formation of $Zn(OH)_2$. Following this, $Zn(OH)_2$ interacts with CO_2 present in the atmosphere to yield $ZnCO_3$. Furthermore, the existence of C and OH^- aids in the development of $Zn_5(OH)_8Cl_2{\cdot}H_2O$.

The findings from the XRD and XPS analyses of the fully immersed samples provide additional insight into the makeup of the corrosion products. Because these corrosion

products are insoluble, they occupy the micropores within the coatings, hindering further interaction between the corrosive environment and the substrate. Consequently, the coatings transition from a state of cathodic protection to one of shielding protection.

4. Conclusions

Based on the commercial 80 WF zinc-rich coating system, the main task of this study was to explore the effect of different concentrations of CNTs on the 80 WF coating, and to evaluate the corrosion protection of the coatings with different concentrations of CNTs for Q355b substrate. Electrochemical testing, salt spray evaluation, SEM, EDS, XRD, XPS, and other evaluation methods were used to study the corrosion resistance of coatings with different concentrations of CNTs. This study provides a valuable reference for the corrosion resistance modification of commercial coatings such as 80 WF, which are mature in the market, and subsequent engineering applications. The following is a summary of the findings of this article:

(1) The 80 WF coating without CNTs demonstrates poor resistance to corrosion, with its overall density being insufficient. In the coating before corrosion, the spherical zinc powder on the surface of the 80 WF coating is not uniformly dispersed, and there is a large gap between adjacent zinc powder. The zinc powder is isolated and cannot be well connected, and the overall coating is not too dense. The zinc powder and corrosion products on the 80 WF coating surface agglomerate after corrosion. Corrosion defects and Fe corrosion products appear, and the overall density of the coating is reduced. In the electrochemical testing, the overall OCP of 80 WF is higher than −0.78 V, indicating that the coating has almost no cathodic protection effect, but mainly plays a protective effect of physical shielding. Moreover, after immersion, the impedance arc in the EIS impedance spectrum is small, the R_{ct} value is smaller, and the i_{corr} of the polarization curve is larger than that of the coatings with 0.3 wt% CNTs. After the salt spray corrosion for 240 h in the salt spray test, obvious corrosion occurred on the surface of the coating, and the matrix corrosion was more serious at the scratch at X, indicating that the cathodic protection ability of the coating was weak.

(2) Compared with 80 WF, the CNTs of the 0.3 wt% CNTs coating adhere stably to the surface of the coating, and the coating surface becomes densified, indicating that CNTs fill the pores between zinc powder particles and epoxy resin to a certain extent, and play a certain shielding role. In addition, the surface morphology shows that CNTs and zinc powder are combined in the coating, which also indicates that CNTs form conductive channels between adjacent spherical zinc powder, which increases the amount of effective activated zinc powder, improves its utilization rate, and enhances the cathodic protection ability of the sacrificial anode of the zinc-rich coating. In the electrochemical testing, the overall OCP of the 0.3 wt% CNTs coating was lower than −0.78 V in the first 14 days, indicating that the coating offered efficient cathodic protection. Moreover, the impedance arc in the EIS spectrum was large, and the R_{ct} value after 28 days of immersion reached 3756 ohms, and the i_{corr} of the polarization curve reached 0.032 A/cm^2, showing its electrochemical properties are better than those of the other five coatings. After salt spray corrosion for 240 h, no obvious corrosion occurred on the surface and the substrate at the scratch of X, indicating that the coating played a cathodic protection role.

(3) With the gradual increase in CNT concentration, a large number of CNTs can be obviously observed on the surface of the 1.0 wt.% CNTs coating. The coating's components are unevenly dispersed, which may adversely affect the basic properties and corrosion resistance of the coating. In the electrochemical testing, the overall OCP of the 1.0 wt.% CNTs coating is higher than −0.78 V, indicating that the coating has almost no cathodic protection effect, but mainly has a protective effect of physical shielding. Moreover, the impedance arc in the EIS spectrum is small, the R_{ct} value is smaller, and the i_{corr} of the polarization curve is larger than that of the 0.3 wt% CNTs coating. After salt spray corrosion for 240 h, a large number of new white corrosion

products were generated on the coating surface in a short period of time, and then serious corrosion occurred in the substrate. Excessive CNTs would adversely affect the corrosion resistance of the coating.

Author Contributions: Formal analysis, X.H. and C.Y.; investigation, J.C. and C.Y.; resources, X.H. and J.C.; experimental research, X.H. and X.Q.; writing—original draft preparation, C.Y. and X.Q.; writing—survey and editing, J.C. and X.Q.; visualization, J.C. and X.H.; supervision, S.Z. and D.S.; project administration, D.S.; funding acquisition, D.S. All authors have read and agreed to the published version of the manuscript.

Funding: This research was funded by the State Grid Jiangsu Electric Power Co., Ltd. Technology Project, grant number J2023009.

Institutional Review Board Statement: Not applicable.

Informed Consent Statement: Not applicable.

Data Availability Statement: Data are included in the article and the corresponding references.

Conflicts of Interest: Authors Xueling Huang, Chun Yang, and Junyu Chen were employed by the State Grid Wuxi Power Supply Company. The remaining authors declare that the research was conducted in the absence of any commercial or financial relationships that could be construed as potential conflicts of interest.

References

1. Munger, C.G.; Vincent, L.D. Corrosion Prevention by Protective Coatings. NACE International 1984. Available online: https://trid.trb.org/View/1165252 (accessed on 5 November 2024).
2. Marchebois, H.; Touzain, S.; Joiret, S.; Bernard, J.; Savall, C. Zinc-rich powder coatings corrosion in sea water: Influence of conductive pigments. *Prog. Org. Coat.* **2002**, *45*, 415–421. [CrossRef]
3. Akbarinezhad, E.; Ebrahimi, M.; Sharif, F.; Attar, M.; Faridi, H. Synthesis and evaluating corrosion protection effects of emeraldine base PAni/clay nanocomposite as a barrier pigment in zinc-rich ethyl silicate primer. *Prog. Org. Coat.* **2011**, *70*, 39–44. [CrossRef]
4. Park, S.; Shon, M. Effects of multi-walled carbon nano tubes on corrosion protection of zinc rich epoxy resin coating. *J. Ind. Eng. Chem.* **2015**, *21*, 1258–1264. [CrossRef]
5. Schaefer, K.; Miszczyk, A. Improvement of electrochemical action of zinc-rich paints by addition of nanoparticulate zinc. *Corros. Sci.* **2013**, *66*, 380–391. [CrossRef]
6. Sørensen, P.A.; Kiil, S.; Dam-Johansen, K.; Weinell, C.E. Anticorrosive coatings: A review. *J. Coat. Technol. Res.* **2009**, *6*, 135–176. [CrossRef]
7. Cubides, Y.; Castaneda, H. Corrosion protection mechanisms of carbon nanotube and zinc-rich epoxy primers on carbon steel in simulated concrete pore solutions in the presence of chloride ions. *Corros. Sci.* **2016**, *109*, 145–161. [CrossRef]
8. Yun, T.H.; Park, J.H.; Kim, J.-S.; Park, J.M. Effect of the surface modification of zinc powders with organosilanes on the corrosion resistance of a zinc pigmented organic coating. *Prog. Org. Coat.* **2014**, *77*, 1780–1788. [CrossRef]
9. Volovitch, P.; Vu, T.; Allély, C.; Aal, A.A.; Ogle, K. Understanding corrosion via corrosion product characterization: II. Role of alloying elements in improving the corrosion resistance of Zn–Al–Mg coatings on steel. *Corros. Sci.* **2011**, *53*, 2437–2445. [CrossRef]
10. Volovitch, P.; Allely, C.; Ogle, K. Understanding corrosion via corrosion product characterization: I. Case study of the role of Mg alloying in Zn–Mg coating on steel. *Corros. Sci.* **2009**, *51*, 1251–1262. [CrossRef]
11. Teng, S.; Gao, Y.; Cao, F.; Kong, D.; Zheng, X.; Ma, X.; Zhi, L. Zinc-reduced graphene oxide for enhanced corrosion protection of zinc-rich epoxy coatings. *Prog. Org. Coat.* **2018**, *123*, 185–189. [CrossRef]
12. Shreepathi, S.; Bajaj, P.; Mallik, B.P. Electrochemical impedance spectroscopy investigations of epoxy zinc rich coatings: Role of Zn content on corrosion protection mechanism. *Electrochim. Acta* **2010**, *55*, 5129–5134. [CrossRef]
13. Shen, L.; Li, Y.; Zhao, W.; Miao, L.; Xie, W.; Lu, H.; Wang, K. Corrosion protection of graphene-modified zinc-rich epoxy coatings in dilute NaCl solution. *ACS Appl. Nano Mater.* **2018**, *2*, 180–190. [CrossRef]
14. Ramezanzadeh, B.; Moghadam, M.M.; Shohani, N.; Mahdavian, M. Effects of highly crystalline and conductive polyaniline/graphene oxide composites on the corrosion protection performance of a zinc-rich epoxy coating. *Chem. Eng. J.* **2017**, *320*, 363–375. [CrossRef]
15. Praveen, B.; Venkatesha, T.; Naik, Y.A.; Prashantha, K. Corrosion studies of carbon nanotubes–Zn composite coating. *Surf. Coat. Technol.* **2007**, *201*, 5836–5842. [CrossRef]
16. Wang, D.; Sikora, E.; Shaw, B. A comparison of the corrosion response of zinc-rich coatings with and without presence of carbon nanotubes under erosion and corrosion conditions. *Corrosion* **2018**, *74*, 1203–1213. [CrossRef] [PubMed]
17. Hammouda, N.; Chadli, H.; Guillemot, G.; Belmokre, K. The corrosion protection behaviour of zinc rich epoxy paint in 3% NaCl solution. *Adv. Chem. Eng. Sci.* **2011**, *1*, 51. [CrossRef]

18. Sofian, A.H.; Tanaka, A.; Noda, K. Corrosion performance of zinc-rich paints (ZRP) on mild steel in NaCl solution. *ECS Trans.* **2013**, *45*, 17. [CrossRef]
19. Li, H.; Duan, J.; Wei, D. Comparison on corrosion behaviour of arc sprayed and zinc-rich coatings. *Surf. Coat. Technol.* **2013**, *235*, 259–266. [CrossRef]
20. Orek, C.; Keser, S.; Kaygili, O.; Zuchowski, P.; Bulut, N. Structures and Optical Properties of Zinc Oxide Nanoclusters: A Combined Experimental and Theoretical Approach. *J. Mol. Model.* **2023**, *29*, 227. [CrossRef] [PubMed]
21. Hoang, N.; Khoa, T.A.; Phuong, P.M.; Hang, T.T.X.; Van Chi, N.; Nguyen, T.D. Corrosion protection of carbon steel using a combination of Zr conversion coating and subsequent zinc-rich silicate coating with a flake ZnAl alloy. *Arab. J. Chem.* **2022**, *15*, 103815. [CrossRef]
22. Hayatdavoudi, H.; Rahsepar, M. A mechanistic study of the enhanced cathodic protection performance of graphene-reinforced zinc rich nanocomposite coating for corrosion protection of carbon steel substrate. *J. Alloys Compd.* **2017**, *727*, 1148–1156. [CrossRef]
23. Ge, T.; Zhao, W.; Wu, X.; Lan, X.; Zhang, Y.; Qiang, Y.; He, Y. Incorporation of electroconductive carbon fibers to achieve enhanced anti-corrosion performance of zinc rich coatings. *J. Colloid Interface Sci.* **2020**, *567*, 113–125. [CrossRef]
24. Fukuda, H.; Szpunar, J.A.; Kondoh, K.; Chromik, R. The influence of carbon nanotubes on the corrosion behaviour of AZ31B magnesium alloy. *Corros. Sci.* **2010**, *52*, 3917–3923. [CrossRef]
25. Pourhashem, S.; Ghasemy, E.; Rashidi, A.; Vaezi, M.R. A review on application of carbon nanostructures as nanofiller in corrosion-resistant organic coatings. *J. Coat. Technol. Res.* **2020**, *17*, 19–55. [CrossRef]
26. Cao, X.; Huang, F.; Huang, C.; Liu, J.; Cheng, Y.F. Preparation of graphene nanoplate added zinc-rich epoxy coatings for enhanced sacrificial anode-based corrosion protection. *Corros. Sci.* **2019**, *159*, 108120. [CrossRef]
27. Bai, W.; Ma, Y.; Meng, M.; Li, Y. The influence of graphene on the cathodic protection performance of zinc-rich epoxy coatings. *Prog. Org. Coat.* **2021**, *161*, 106456. [CrossRef]
28. Rastogi, R.; Kaushal, R.; Tripathi, S.; Sharma, A.L.; Kaur, I.; Bharadwaj, L.M. Comparative study of carbon nanotube dispersion using surfactants. *J. Colloid Interface Sci.* **2008**, *328*, 421–428. [CrossRef]
29. Pandey, P.; Mohanty, S.; Nayak, S.K. Tailoring dispersion and interaction of MWNT in polymer nanocomposites, using Triton X-100 as nonionic surfactant. *J. Mater. Eng. Perform.* **2014**, *23*, 4385–4393. [CrossRef]
30. Husanu, M.; Baibarac, M.; Baltog, I. Non-covalent functionalization of carbon nanotubes: Experimental evidence for isolated and bundled tubes. *Phys. E Low-Dimens. Syst. Nanostruct.* **2008**, *41*, 66–69. [CrossRef]
31. Pereyra, A.; Giudice, C.; Herrera, L.K.; Echeverría, F.; Castano, J.G. Tripigmented anticorrosive coatings based on lamellar zinc as inhibitor. *Surf. Coat. Int.* **2006**, *89*, 245–249. [CrossRef]
32. Knudsen, O.Ø.; Steinsmo, U.; Bjordal, M. Zinc-rich primers—Test performance and electrochemical properties. *Prog. Org. Coat.* **2005**, *54*, 224–229. [CrossRef]
33. Kalendová, A. Effects of particle sizes and shapes of zinc metal on the properties of anticorrosive coatings. *Prog. Org. Coat.* **2003**, *46*, 324–332. [CrossRef]
34. Jalili, M.; Rostami, M.; Ramezanzadeh, B. An investigation of the electrochemical action of the epoxy zinc-rich coatings containing surface modified aluminum nanoparticle. *Appl. Surf. Sci.* **2015**, *328*, 95–108. [CrossRef]
35. Gergely, A.; Pászti, Z.; Mihály, J.; Drotár, E.; Török, T. Galvanic function of zinc-rich coatings facilitated by percolating structure of the carbon nanotubes. Part I: Characterization of the nano-size particles. *Prog. Org. Coat.* **2015**, *78*, 437–445. [CrossRef]
36. Xu, L.; Liu, F.; Wang, Z.; Ke, W.; Han, E.-H.; Jie, G.; Wang, J.; Huang, H. The effect of surface modification of zinc particles with phosphoric acid on the corrosion resistance of cold galvanizing coatings. *Prog. Org. Coat.* **2018**, *114*, 90–101. [CrossRef]
37. Hu, J.-M.; Zhang, J.-T.; Zhang, J.-Q.; Cao, C.-N. A novel method for determination of diffusion coefficient of corrosive species in organic coatings by EIS. *J. Mater. Sci.* **2004**, *39*, 4475–4479. [CrossRef]
38. Cubides, Y.; Su, S.S.; Castaneda, H. Influence of zinc content and chloride concentration on the corrosion protection performance of zinc-rich epoxy coatings containing carbon nanotubes on carbon steel in simulated concrete pore environments. *Corrosion* **2016**, *72*, 1397–1423. [CrossRef]
39. Amirudin, A.; Thieny, D. Application of electrochemical impedance spectroscopy to study the degradation of polymer-coated metals. *Prog. Org. Coat.* **1995**, *26*, 1–28. [CrossRef]
40. Wang, F.; Feng, L.; Huang, Y.; Shen, W.; Ma, H. Effect of the gradient distribution of multiwalled carbon nanotubes on the bond strength and corrosion resistance of waterborne polyurethane conductive nanocomposites. *Prog. Org. Coat.* **2020**, *140*, 105507. [CrossRef]
41. Li, A.; Sun, M.; Ma, Z.; Chen, S.; Zhu, G.; Zhang, Y.; Wang, W. Anticorrosion performance of polyvinyl butyral composite coatings improved by polyaniline-multiwalled carbon nanotubes/poly (methylhydrosiloxane). *Thin Solid Films* **2020**, *712*, 138347. [CrossRef]